Petrology, geochemistry

New U-Pb zircon and ^{40}Ar/^{39}Ar muscovite age constraints on the emplacement of the Lizio syn-tectonic granite (Armorican Massif, France)

Nouveaux âges U-Pb sur zircon et ^{40}Ar/^{39}Ar sur muscovite de mise en place du granite syn-tectonique de Lizio (Massif Armoricain, France)

Romain Tartèse [a,*], Marc Poujol [a], Gilles Ruffet [a,b], Philippe Boulvais [a], Philippe Yamato [a], Jan Košler [c]

[a] UMR CNRS 6118 géosciences, université de Rennes 1, 35042 Rennes cedex, France
[b] CNRS (CNRS/INSU), UMR 6118, géosciences Rennes, 35042 Rennes cedex, France
[c] Department of Earth Science and Centre for Geobiology, University of Bergen, 5007 Bergen, Norway

ARTICLE INFO

ABSTRACT

LA-ICP-MS U-Pb analyses performed on zircon grains from the Lizio granite yielded an emplacement age of 316 ± 6 Ma. Typical S-C structures show that the Lizio granite was emplaced contemporaneously with dextral shearing along the northern branch of the South Armorican Shear Zone and that it was therefore active at that time. ^{40}Ar/^{39}Ar analyses performed on muscovite grains yielded plateau dates ranging between 311.5 and 308.2 Ma. Muscovite chemistry is typical of primary magmatic muscovite, which precludes a late fluids-induced resetting of the K-Ar isotopic system. ^{40}Ar/^{39}Ar dates thus likely correspond to the cooling ages below the argon closure temperature. Considering the uncertainties on the measured ages, we can propose that either the Lizio granite cooled down quickly in less than a million of years or that it remained in a hot environment for several millions of years after its emplacement. This latter scenario could have been sustained by shear heating during dextral shearing along the northern branch of the South Armorican Shear Zone.

© 2011 Académie des sciences. Published by Elsevier Masson SAS. All rights reserved.

RÉSUMÉ

Les analyses U-Pb réalisées sur des zircons du granite de Lizio par LA-ICP-MS ont livré un âge de mise en place de 316 ± 6 Ma. Des structures C-S caractéristiques démontrent que le granite de Lizio s'est mis en place pendant le cisaillement dextre le long de la branche nord du Cisaillement Sud Armoricain, qui était donc toujours actif à cette époque. Les analyses ^{40}Ar/^{39}Ar réalisées sur les muscovites ont donné des âges plateaux allant de 311,5 à 308,2 Ma. La chimie des muscovites est typique de celle d'une muscovite magmatique primaire, ce qui écarte une remise à zéro tardive, induite par des fluides, du système isotopique K-Ar. Ces dates ^{40}Ar/^{39}Ar correspondent donc probablement à des âges de refroidissement sous la température de fermeture de l'argon. En tenant compte des incertitudes sur les âges obtenus, cela implique, soit un refroidissement rapide du granite de Lizio en moins d'un million d'années, soit que le granite est resté dans un environnement chaud pendant plusieurs millions d'années après sa mise en place, grâce à la chaleur frictionnelle produite pendant le cisaillement dextre le long du Cisaillement Sud Armoricain.

© 2011 Académie des sciences. Publié par Elsevier Masson SAS. Tous droits réservés.

---

* Corresponding author.
 E-mail address: romain.tartese@univ-rennes1.fr (R. Tartèse).

1. Introduction

In the continental crust, granitic plutons emplace at different stages during the evolution of an orogen. In the Armorican Variscan belt, numerous peraluminous granites were emplaced during the Carboniferous (e.g. Bernard-Griffiths et al., 1985). Most of these granites are spatially associated with the dextral lithospheric-scale South Armorican Shear Zone (SASZ). Moreover, emplacement of these granites is often coeval with shearing as indicated by the S-C structures they display (Berthé et al., 1979; Gapais, 1989). The precise dating of these synkinematic granites and of their cooling history is therefore an essential tool to place time constraints on the different tectono-thermal events that occur during the life of the Variscan orogen.

So far, available geochronological data on the emplacement of these granites are solely provided by whole rock Rb-Sr isochron ages (Bernard-Griffiths et al., 1985; Peucat et al., 1979). Along the northern branch of the SASZ, three granitic massifs are assumed to have emplaced synkinematically around 344–337 ± 13–8 Ma, which implies that the shear zone was active during the Lower Visean. In order to better constrain dextral shearing along the northern branch of the SASZ, we have performed new zircon U-Pb and muscovite ^{40}Ar/^{39}Ar datings.

2. Geological framework

During Variscan times, the Armorican Massif has undergone deformation related to a major continental collision between Gondwana and Laurussia (e.g. Ballèvre et al., 2009). This episode was followed by the development of dextral shear zones that can be traced over a distance of a couple of hundred of kilometres, namely the North Armorican Shear Zone (NASZ) and the SASZ (Fig. 1a). The SASZ separates two distinct domains within the Armorican Massif that are characterized by contrasted metamorphic and structural histories. To the south, the South Armorican domain (SAD) is mainly composed of deep crustal units (medium to high-grade micaschists, migmatitic gneisses and anatectic granites) that have been exhumed during the extension associated with the chain collapse (e.g. Brown and Dallmeyer, 1996; Gapais et al., 1993; Turrillot et al., 2009). To the north, the central Armorican domain (CAD) is made of a Late Proterozoic–
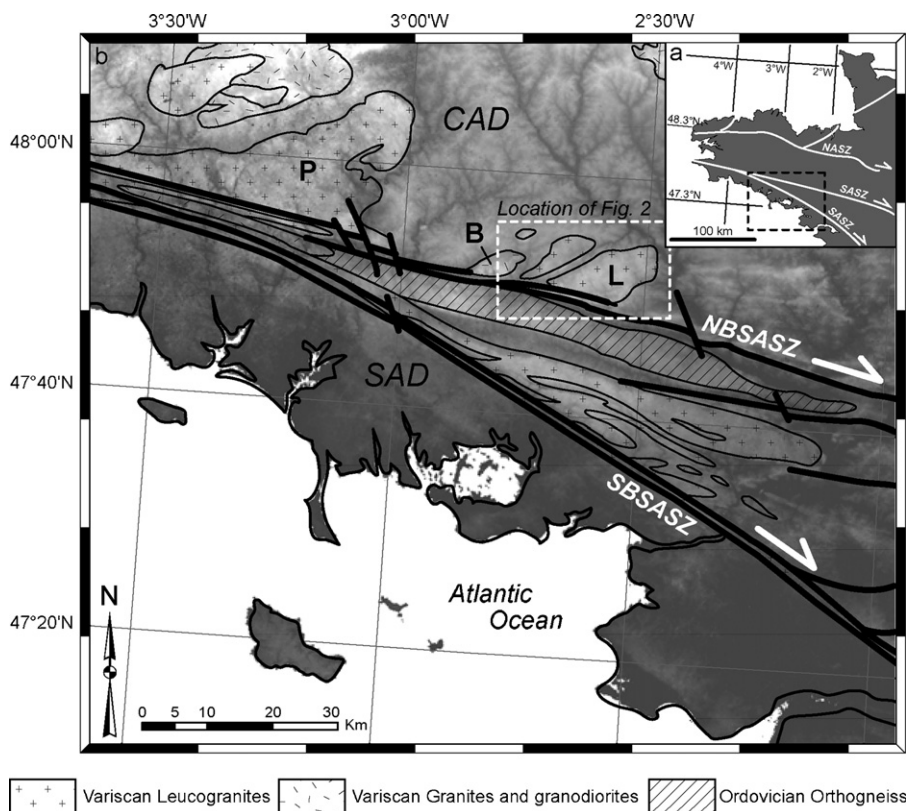

Fig. 1. (a) Location of the studied area in the Armorican Massif. NASZ: North Armorican Shear Zone; SASZ: South Armorican Shear Zone. (b) Simplified geological map of the studied area showing the plutonic intrusions. NBSASZ and SBSASZ are the northern and southern branches of the South Armorican Shear Zone, respectively. P, B and L are the Pontivy, Bignan and Lizio granites, respectively. CAD and SAD are the central and South Armorican domains, respectively.

Fig. 1. (a) Localisation de la zone d'étude dans le Massif Armoricain. NASZ: Cisaillement Nord-Armoricain; SASZ : Cisaillement Sud-Armoricain. (b) Carte géologique simplifiée de la zone d'étude représentant les intrusions plutoniques. NBSASZ et SBSASZ sont respectivement les branches nord et sud du Cisaillement Sud Armoricain. P, B et L sont les granites de Pontivy, Bignan et Lizio, respectivement. CAD et SAD sont respectivement les domaines centre et Sud Armoricain.
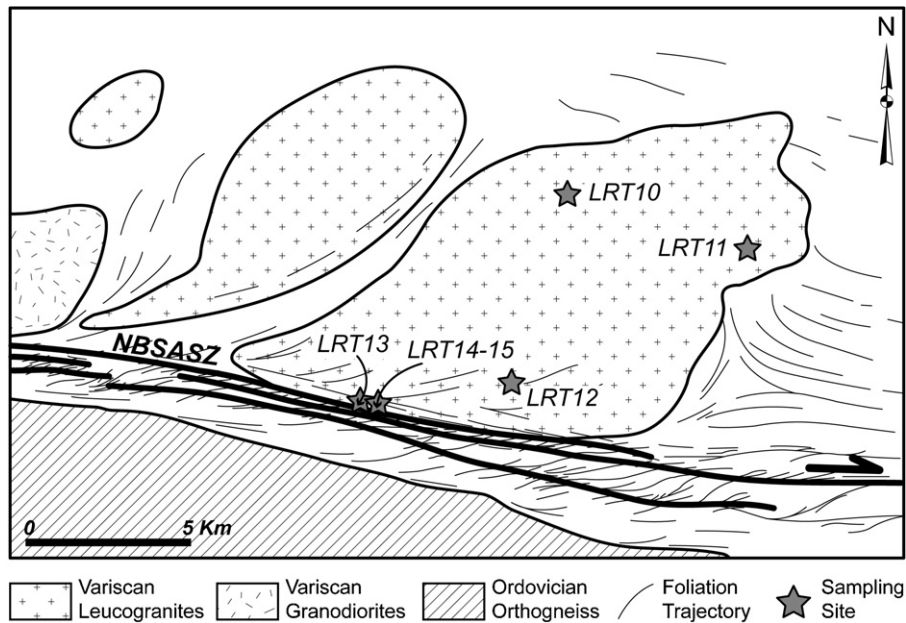
Fig. 2. Simplified geological map of the Lizio granite (after Berthé, 1980).

Fig. 2. Carte géologique simplifiée du granite de Lizio (d'après Berthé, 1980).

Early Palaeozoic sedimentary succession, which has been affected by low-grade metamorphism (e.g. Le Corre et al., 1991). In the CAD, both strain intensity (Gumiaux et al., 2004), metamorphic degree (Le Corre et al., 1991) and evidence of fluid flow (Gloaguen et al., 2007; Lemarchand et al., 2011) increase southward reaching a maximum on the SASZ itself.

The SASZ is geometrically defined by ca. 100–1000 m wide zone of highly strained mylonitic rocks (Jégouzo, 1980; Tartèse et al., 2011a). In details, the SASZ is divided into two main branches (Fig. 1a). In the southern branch network (SBSASZ), the mylonitic foliation bears a 5–10° eastward dipping stretching lineation. Along this branch, a dextral displacement of ca. 150 to 200 km has been proposed based on the width of the mylonitized rocks (Jégouzo and Rossello, 1988). The northern branch (NBSASZ) is sublinear and extends for about 300 km. It displays a subvertical mylonitic foliation also bearing a stretching lineation dipping at ca. 10° eastward. Along this branch, a 40 km minimal dextral offset has been estimated from geometrical reconstructions (Jégouzo and Rossello, 1988).

The Lizio two-mica granite was emplaced along the NBSASZ (Fig. 1b). This granitic massif is highly emblematic because it represents the *locus typicus* where S-C structures were first described as resulting from a single deformational event (Berthé et al., 1979). These structures indicate that the Lizio granite was emplaced during shearing along the NBSASZ. Indeed, "S-planes" correspond to shearing planes which localized the dextral deformation. These "S-planes" are vertical and their orientation mimics that of the NBSASZ. "C-planes" correspond to cleavage planes. These "C-planes" rotate during non-coaxial shearing. They define an angle of around 45° with "S-planes" in slightly deformed samples, angle which decreases with increasing

strain until parallelisation of "S-planes" and "C-planes" in ultramylonitized samples (Berthé et al., 1979). According to Gapais (1989), these S-C structures developed during cooling of intrusives at temperatures around 550 °C. The synkinematic characteristics of the Lizio granite emplacement are also evidenced by the triple-point defined by the foliation around the intrusion (Fig. 2). This triple-point formed by the combination of the regional stress and the stress related to the granite emplacement.

Whole rock Rb-Sr data obtained on the Lizio granite define a 338 ± 13 Ma isochron age (2σ) interpreted as the granite emplacement age (Peucat et al., 1979). This age is similar within error to the 344 ± 8 Ma and 337 ± 13 Ma ages (2σ) obtained by these authors on the Pontivy and Bignan synkinematic massifs, both located a couple of kilometres westward and also rooted into the NBSASZ (Fig. 1b). More recently, a zircon U-Pb emplacement age of 316 +5/–3 Ma (ID-TIMS, Béchennec et al., 2001) has been obtained on the St-Thurien metagranite ca. 250 m south of the NBSASZ (3°40'23"W; 47°57'50"N). This St-Thurien metagranite is highly sheared and displays characteristic S-C structures, with subvertical "S-planes" and "C-planes" oriented N105-110° and ca. N080°, respectively (Béchennec et al., 2001). The St-Thurien metagranite is thus synkinematic with dextral shearing along the NBSASZ, which indicates that shearing continued after 330–325 Ma.

The geochemistry of the Lizio two-mica granite has been studied in details by Tartèse and Boulvais (2010). This study provided mineral and whole rock geochemical data as well as new Rb-Sr, Sm-Nd and O isotope data which are consistent with the few data published by Bernard-Griffiths et al. (1985). The Lizio granite is highly silicic, poor in ferromagnesian and was formed by partial melting of a metasedimentary source. Geochemical data show that

a subtle magmatic differentiation occurred by crystal fractionation from the melt (Tartèse and Boulvais, 2010). Finally the Lizio granite intruded Brioverian metapelites of the CAD. During its emplacement in the Brioverian metapellites, a syntectonic paragenesis of Bt + Ms + Chl + St + Grt ± And developed (Berthé, 1980; mineral abbreviations are after Whitney and Evans, 2010), corresponding to the facies 2b of Pattison and Tracy (1991) and to a pressure of around 4 kbar (Pattison et al., 1999).

3. Samples description

3.1. Petrography

A full petrographic description of the samples presented in this study, as well as mineral and whole-rock geochemical data, and oxygen isotope data are given in Tartèse and Boulvais (2010). To summarize, in the Lizio two-mica granite, quartz and feldspar (orthoclase, microcline and plagioclase) represent around 90% of the mineral assemblage (Fig. 3) while biotite and muscovite represent the remaining 10%, biotite being generally more abundant than muscovite. Accessory minerals are apatite, zircon and monazite.

In undeformed samples, quartz is large and often euhedral (Fig. 3a–b) whereas it is recrystallized in ribbons in deformed samples (Fig. 3c–d). Plagioclase is euhedral to subeuhedral and shows thin polysynthetic twinning. Alkali

feldspar is generally subeuhedral. Microcline and orthoclase generally displays well-expressed tartan and Carlsbad twinning, respectively. Pleochroic biotite forms euhedral brown-reddish flakes (Fig. 3a–b) and hosts most of the accessory minerals (Fig. 3b). Muscovite usually forms large flakes, some of them having a fish-like habit due to shearing (Fig. 3c). In deformed samples, shear bands are usually localized in small biotite and muscovite grains aggregates (Fig. 3c–d).

3.2. Mineral chemistry

Analytical procedure for electron microprobe analysis of minerals are detailed in Pitra et al. (2008) and Tartèse and Boulvais (2010). K-feldspar is close to the orthose end-member (Or = 91–92 mol.%) and plagioclase is albite on average (Ab = 91 mol.%). Biotite composition is homogeneous in the investigated samples and typical of peraluminous granites (Tartèse and Boulvais, 2010). Concerning muscovite, complementary electron microprobe data have been acquired, compared to the dataset published in Tartèse and Boulvais (2010), as muscovite is the mineral chosen for $^{40}Ar/^{39}Ar$ dating in this study. Only data obtained on large muscovite phenocrysts are reported in Table 1 and displayed in Fig. 4. Muscovite grains have a homogeneous chemical composition with FeO = 1.1–1.4 wt.%, MgO = 0.8–0.9 wt.% and Na$_2$O = 0.5–0.7 wt.% (Table 1). They also have a high TiO$_2$ content (0.6–
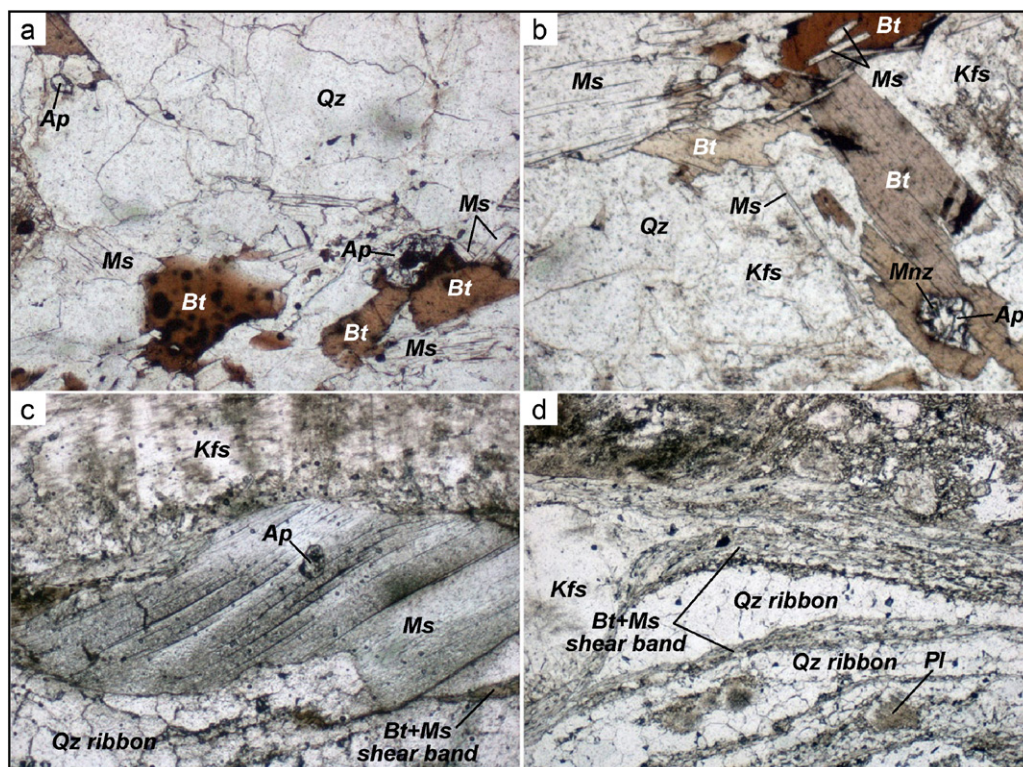
Fig. 3. Photomicrographs showing the typical structures of the Lizio granite samples, from undeformed (a and b) to mylonitized (c and d). Mineral abbreviations are after Whitney and Evans (2010).

Fig. 3. Microphotographies montrant les structures typiques des échantillons du granite de Lizio, depuis les échantillons non déformés (a et b) jusqu'aux échantillons mylonitisés (c et d). Les abréviations des minéraux sont celles de Whitney et Evans (2010).

Table 1
Average chemical compositions of muscovite.

Tableau 1
Compositions chimiques moyennes des muscovites.

	MUSCOVITE									
	LRT15 ($n=16$)	sd	LRT10 ($n=19$)	sd	LRT11 ($n=10$)	sd	LRT12 ($n=14$)	sd	LRT14 ($n=15$)	sd
SiO_2	46.5	0.3	45.7	0.4	46.4	0.2	45.7	0.5	46.1	0.3
TiO_2	1.1	0.2	0.7	0.2	0.6	0.2	1.1	0.2	1.0	0.2
Al_2O_3	34.5	0.2	35.8	0.3	35.0	0.3	34.7	0.5	34.9	0.4
FeO	1.4	0.1	1.1	0.1	1.2	0.2	1.3	0.1	1.4	0.1
MgO	0.9	0.1	0.8	0.1	0.8	0.1	0.8	0.1	0.8	0.1
Na_2O	0.5	0.1	0.7	0.1	0.6	0.1	0.5	0.1	0.5	0.1
K_2O	11.0	0.2	10.8	0.2	10.7	0.6	11.2	0.3	11.1	0.2
SUM	95.8		95.6		95.3		95.4		95.8	
Structural formula based on 22 oxygen atoms										
Si	6.17	0.02	6.08	0.02	6.17	0.03	6.11	0.04	6.13	0.02
Ti	0.11	0.02	0.07	0.02	0.06	0.02	0.11	0.02	0.10	0.02
Al	5.40	0.03	5.61	0.03	5.49	0.03	5.48	0.06	5.47	0.05
Fe	0.16	0.01	0.13	0.01	0.14	0.02	0.15	0.01	0.15	0.01
Mg	0.18	0.01	0.15	0.01	0.15	0.02	0.16	0.02	0.17	0.02
Na	0.12	0.02	0.19	0.03	0.15	0.04	0.14	0.03	0.14	0.03
K	1.86	0.04	1.84	0.04	1.83	0.09	1.91	0.04	1.88	0.03
SUM	14.00		14.06		13.99		14.06		14.04	

Oxide contents in wt.% and cationic contents in apfu. sd: standard deviation.

1.1 wt.% on average, Table 1) and consistently fall in the primary magmatic muscovite field in the Mg-Ti-Na ternary diagram (Miller et al., 1981; Fig. 4a). In the Mg + Fe against Si plot (Fig. 4b), muscovite analyses are clustered showing that limited phengitic substitution occurred in the studied samples.

4. Geochronological results

4.1. Zircon U-Pb dating

Zircon U-Pb data were obtained in situ by laser ablation inductively coupled plasma mass spectrometry (LA-ICP-MS) performed at the Centre for Element and Isotope Analysis, University of Bergen, Norway. A classical mineral separation procedure has been followed to concentrate zircon grains suitable for U-Pb dating from samples LRT10,

LRT12 and LRT15, these three samples representing undeformed, deformed and mylonitized end-members in the rock collection. Rocks were crushed and the powder fractions with a diameter < 250 μm have been isolated. Heavy minerals were successively concentrated by Wilfley table and heavy liquids procedures. Magnetic minerals were then removed with an isodynamic Frantz separator. Zircon grains were carefully examined under a binocular microscope, selected, and embedded in epoxy mounts. Then grains were hand-grounded and polished on a lap wheel with 6 μm and 1 μm diamond suspension successively. They were imaged in transmitted and reflected light, and their internal structure has been revealed using SEM BSE imaging at the LaSalle Institute, Beauvais, France.

Before analysis, grain mounts were cleaned using a weak HNO_3 solution and rinsed several times using Millipore water and ethanol in an ultrasonic bath. They
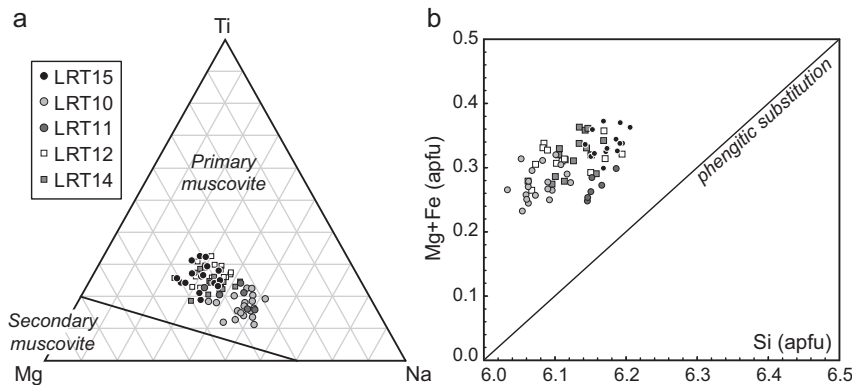

Fig. 4. (a) Muscovite chemical compositions plotted in the ternary Mg-Ti-Na diagram of Miller et al. (1981). (b) Mg + Fe (apfu) vs. Si (apfu) content of muscovite showing the extent of phengitic substitution.

Fig. 4. (a) Compositions chimiques des muscovites représentées dans le diagramme ternaire Mg-Ti-Na de Miller et al. (1981). (b) Teneurs Mg + Fe (apfu) vs. Si (apfu) des muscovites illustrant l'étendue de la substitution phengitique.
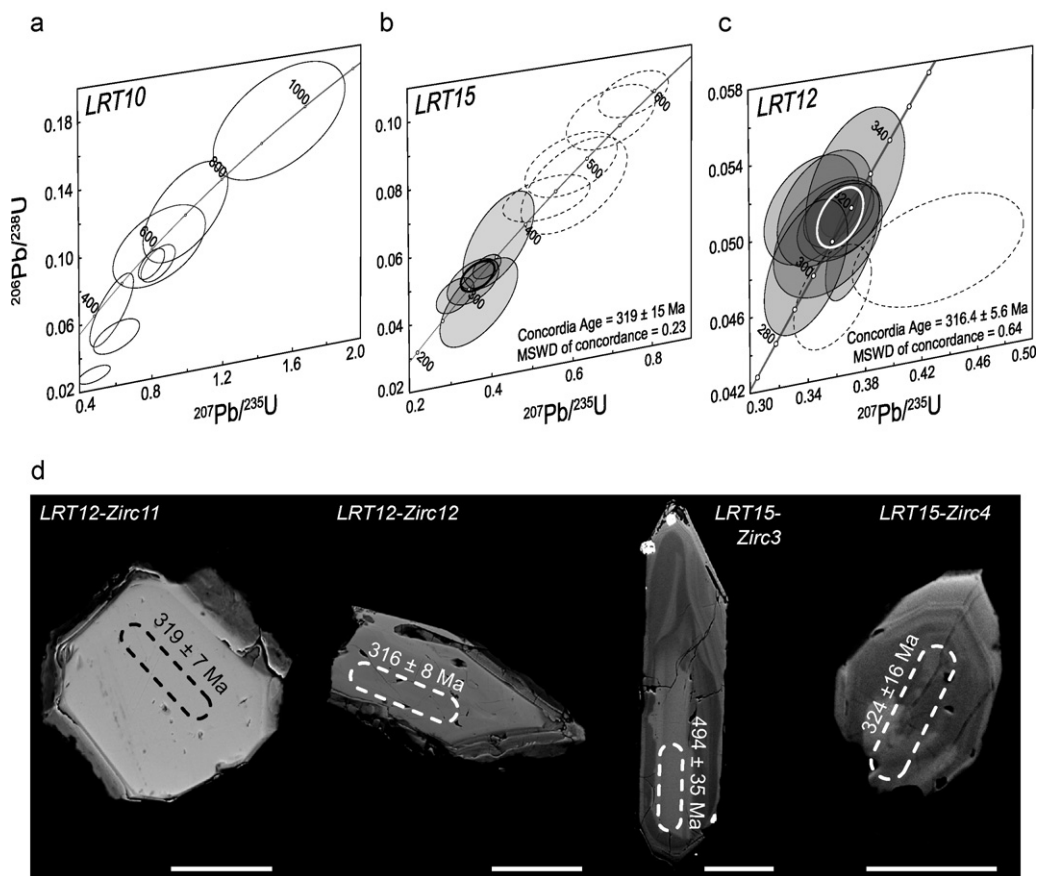
Fig. 5. (a) Wetherill concordia diagram for zircon data from the sample LRT10. (b) Wetherill concordia diagram for zircon data from the sample LRT15. (c) Wetherill concordia diagram for zircon data from the sample LRT12. In these diagrams, error ellipses are at 1σ. Concordia ages have been calculated with the ellipses in grey and include decay constants errors. (d) SEM BSE images of zircon grains from samples LRT12 and LRT15 with LA-ICP-MS analyzed rasters (dotted zones) and obtained ^{206}Pb/^{238}U dates. For all the grains, the scale bar represents 50 μm.

Fig. 5. (a) Diagramme concordia Wetherill pour les données des zircons de l'échantillon LRT10. (b) Diagramme concordia Wetherill pour les données des zircons de l'échantillon LRT15. (c) Diagramme concordia Wetherill pour les données des zircons de l'échantillon LRT12. Dans ces diagrammes, les ellipses d'incertitude sont à 1σ. Les âges concordia ont été calculés avec les ellipses en gris et incluent les incertitudes sur les constantes de désintégration. (d) Images MEB rétrodiffusées de grains de zircon des échantillons LRT12 et LRT15, avec les zones analysées (en pointillés) par LA-ICP-MS et les dates ^{206}Pb/^{238}U obtenues. L'échelle représente 50 μm pour tous les grains.

were then mounted in the laser ablation cell together with several standards for quality control. A 213 Nd-YAG laser (New Wave UP-213) was used coupled to a single-collector, double focusing magnetic sector ICP-MS system (Thermo Finnigan Element 2). Data have been plotted in Wetherill concordia diagrams using the software Isoplot/ Ex (Ludwig, 2008). In Fig. 5, data are plotted with their uncertainties at 1σ. Results are reported in the Table 2 where uncertainties are listed at 1σ. When ages are calculated, all errors are reported at the 2σ confidence level.

Zircon grains were ablated using a laser beam of ca. 15 μm in diameter that was rastered over the sample surface to create a line of ca. 50 μm in length depending on the grain size. The laser energy was set at 5 J.cm^{-2} with a repetition rate of 10 Hz. Together with the sample introduction, the system allowed the simultaneous nebulization of an internal standard tracer solution following the technique described by Košler et al. (2002) and Košler

and Sylvester (2003). Zircon data were collected on unknown zircon grains and three zircon standards, 91500 (1065 Ma; Wiedenbeck et al., 1995), Plešovice (337 Ma; Sláma et al., 2008) and GJ-1 (609 Ma; Jackson et al., 2004). Typically 10–15 unknowns were collected for every 7 analyses of the standards. Analysing and treating the zircon standards as unknowns is a robust quality control procedure that allows assessment of the accuracy and precision of the technique during an analytical session. Analyses done on the Plešovice and GJ-1 zircon standards yielded concordant ages of 335 ± 4 Ma ($n = 12$; MSWD = 1.13) and 603 ± 11 Ma ($n = 9$; MSWD = 0.30). Raw data were processed offline using an Excel spreadsheet-based program (Lamdate; Košler et al., 2008).

BSE images of zircon grains from sample LRT12 revealed unzoned grey cores surrounded by thin darker rims, without evidence of inherited cores (Fig. 5d). In sample LRT15, zircon grains display a more pronounced oscillatory zoning where dark cores are surrounded by

Table 2
Zircon U-Pb isotopic data. All uncertainties are at 1σ.

Tableau 2
Données isotopiques U-Pb sur zircon. Les incertitudes sont à 1σ.

Sample, grain, spot	Isotopic ratios						Rho	Calculated ages (Ma)					
	$^{207}Pb/^{235}U$	±	$^{206}Pb/^{238}U$	±	$^{207}Pb/^{206}Pb$	±		$^{206}Pb/^{238}U$	±	$^{207}Pb/^{235}U$	±	$^{207}Pb/^{206}Pb$	±
LRT10 - Zircon													
Zirc1.2	0.8456	0.1709	0.0986	0.0150	0.0618	0.0063	0.38	606	88	622	94	667	220
Zirc2.1	1.5298	0.2502	0.1619	0.0217	0.0695	0.0065	0.41	967	120	942	100	915	192
Zirc3.1	0.8374	0.0634	0.0885	0.0067	0.0729	0.0084	0.50	547	40	618	35	1011	233
Zirc4.1	0.5790	0.0799	0.0656	0.0134	0.0634	0.0082	0.74	410	81	464	51	723	275
Zirc5.1	0.9942	0.1581	0.1165	0.0185	0.0581	0.0065	0.50	710	107	701	81	532	245
Zirc7.1	0.6049	0.0842	0.0494	0.0061	0.0891	0.0086	0.45	311	38	480	53	1406	184
Zirc7.2	0.8016	0.0485	0.0889	0.0057	0.0612	0.0031	0.53	549	33	598	27	645	107
Zirc8.1	0.4803	0.0583	0.0290	0.0031	0.1430	0.0120	0.44	184	19	398	40	2264	145
LRT12 - Zircon													
Zirc2.1	0.4324	0.0406	0.0478	0.0019	0.0664	0.0051	0.21	301	11	365	29	819	159
Zirc4.1	0.3640	0.0102	0.0509	0.0009	0.0507	0.0014	0.33	320	6	315	8	227	65
Zirc5.1	0.3711	0.0125	0.0490	0.0019	0.0538	0.0015	0.59	308	12	320	9	363	62
Zirc6.1	0.3542	0.0251	0.0495	0.0020	0.0528	0.0032	0.29	312	12	308	19	320	138
Zirc7.1	0.3429	0.0219	0.0511	0.0018	0.0501	0.0021	0.28	322	11	299	17	198	100
Zirc8.1	0.3519	0.0218	0.0511	0.0019	0.0503	0.0022	0.31	321	12	306	16	211	102
Zirc8.2	0.3734	0.0230	0.0522	0.0025	0.0527	0.0022	0.39	328	15	322	17	315	93
Zirc9.1	0.3571	0.0179	0.0463	0.0018	0.0562	0.0026	0.38	292	11	310	13	460	102
Zirc11.1	0.3618	0.0162	0.0507	0.0011	0.0524	0.0023	0.25	319	7	314	12	302	101
Zirc12.1	0.3616	0.0191	0.0502	0.0013	0.0540	0.0022	0.24	316	8	313	14	373	91
Zirc13.1	0.3387	0.0192	0.0481	0.0023	0.0524	0.0016	0.42	303	14	296	15	303	71
LRT15 - Zircon													
Zirc1.1	0.4161	0.0578	0.0607	0.0090	0.0516	0.0056	0.53	380	54	353	41	268	250
Zirc2.1	0.3675	0.0629	0.0431	0.0080	0.0608	0.0096	0.54	272	50	318	47	634	338
Zirc3.1	0.5965	0.0759	0.0796	0.0059	0.0548	0.0039	0.29	494	35	475	48	405	161
Zirc3.2	0.6041	0.0876	0.0732	0.0088	0.0598	0.0077	0.42	455	53	480	55	596	280
Zirc4.1	0.3682	0.0297	0.0515	0.0026	0.0515	0.0034	0.32	324	16	318	22	262	153
Zirc5.1	0.3531	0.0417	0.0496	0.0042	0.0524	0.0054	0.36	312	26	307	31	304	237
Zirc5.2	0.3871	0.0229	0.0533	0.0022	0.0537	0.0026	0.35	335	13	332	17	357	111
Zirc6.1	0.7527	0.0583	0.0977	0.0042	0.0589	0.0021	0.28	601	25	570	34	564	79
Zirc7.1	0.5352	0.0713	0.0707	0.0041	0.0581	0.0054	0.22	440	25	435	47	533	204
Zirc8.1	0.3093	0.0302	0.0464	0.0032	0.0502	0.0025	0.36	292	20	274	23	204	115
Zirc9.1	0.6964	0.0739	0.0918	0.0059	0.0555	0.0031	0.30	566	35	537	44	432	125

brighter rims (Fig. 5d). Some zircon grains also contain small monazite inclusions (for example in LRT15-Zirc3 in Fig. 5d). In sample LRT10, two analyses are largely discordant and yield therefore meaningless dates (Fig. 5a). From the remaining concordant analyses, one yields a date of ca. 950 Ma, and another five dates are grouped around 600–500 Ma (Fig. 5a). In sample LRT15, the complete dataset of 11 analyses plot in a concordant to subconcordant position (Fig. 5b). Among them, six define an imprecise concordia age of 319 ± 15 Ma (MSWD = 0.23). The five remaining datapoints define dates between ca. 600 and 450 Ma. Finally, in sample LRT12, eleven analyses have been performed (Table 2). When plotted in a Wetherill concordia diagram (Fig. 5c), nine datapoints define a concordia age of 316.4 ± 5.6 Ma (MSWD = 0.64), identical within error with the age recorded by sample LRT15 but more precise.

4.2. Muscovite $^{40}Ar/^{39}Ar$ dating

Euhedral to subeuhedral single grains of muscovite, with variably deformed shapes, were handpicked from the 0.25–1.50 mm fraction. Irradiation was performed at the McMaster reactor (Hamilton, Canada) and lasted 43.33 hr

(total fluence of 2.6×10^{18} n.cm^{-2}). It was monitored with Taylor Creek Rhyolite (TCR-2) sanidine (28.34 Ma, Renne et al., 1998). Muscovite single grains were analyzed by step-heating with a $^{40}Ar/^{39}Ar$ laser probe, following the procedure described in Ruffet et al. (1991, 1995). Blanks were performed routinely each first or third step, and subtracted from subsequent sample gas fractions. A plateau age is obtained when apparent ages of at least three consecutive steps, representing a minimum of 70% of the ^{39}Ar released, agree within 2σ error bars with the integrated age of the plateau segment. The $^{40}Ar/^{39}Ar$ analytical data are portrayed as age spectra in Fig. 6. All reported uncertainties both in the Fig. 6 and in the text are at the 2σ confidence level.

Single muscovite grains have been analyzed in four samples from the Lizio granite (LRT10, LRT11, LRT13 and LRT15). These samples yielded plateau dates ranging between 311.5 ± 0.4 Ma down to 308.2 ± 0.6 Ma (Fig. 6). They display slight saddle-shaped $^{40}Ar/^{39}Ar$ age spectra that might reflect slight perturbations of the K-Ar isotopic system (e.g. Alexandrov et al., 2002; Cheilletz et al., 1999). An important point is that there is no relationship between the obtained dates and the shearing gradient observed throughout the Lizio granite.
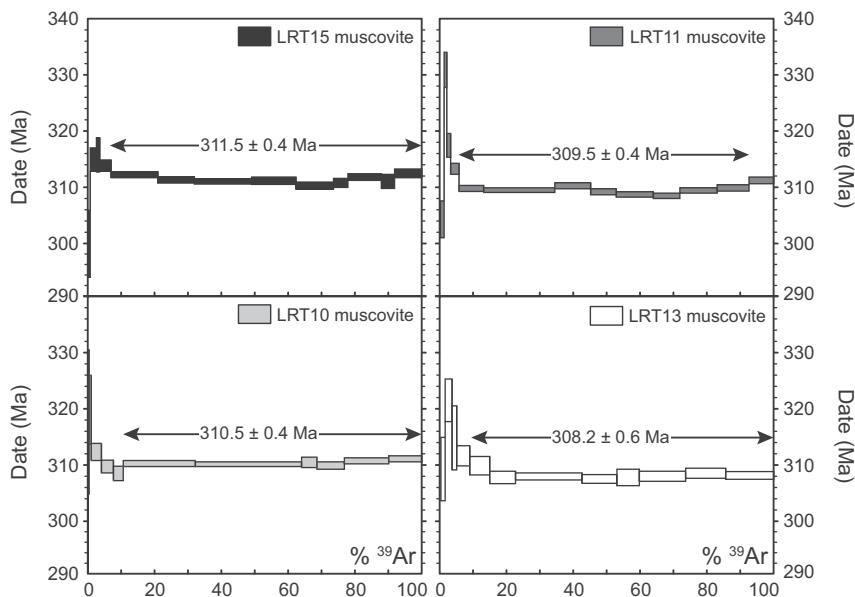
Fig. 6. $^{40}Ar/^{39}Ar$ age spectra of analyzed muscovites. The age error bars for each temperature steps are at the 1σ level. The errors in the J-values are not included. Plateau ages are given with a 2σ uncertainty.

Fig. 6. Spectres d'âges $^{40}Ar/^{39}Ar$ des muscovites analysées. Pour chaque étape de température, les barres d'erreur sur les âges sont à 1σ. Les incertitudes sur les facteurs-J ne sont pas incluses. Les âges plateaux sont donnés avec une incertitude à 2σ.

5. Interpretation and discussion

Considering the high closure temperature for the U-Pb radiogenic system in zircon in excess of 800 °C (Cherniak and Watson, 2001), we interpret the age of 316 ± 6 Ma obtained on sample LRT12 from the synkinematic Lizio granite as its emplacement age along the NBSASZ. The age of 319 ± 15 Ma obtained on sample LRT15 is imprecise but consistent with this emplacement age. Older dates obtained on zircon grains from samples LRT10 and LRT15 illustrate the classical phenomenon of inheritance which often characterizes granitic rocks (e.g. Bea et al., 2007; Harrison et al., 1987; Miller et al., 2003; Roddick and Bevier, 1995). Here, inherited dates mainly range between Neo-Proterozoic and Upper Ordovician times. Concerning the emplacement age of 316 ± 6 Ma, it is identical to the zircon U-Pb emplacement age of 316 +5/−3 Ma of the St-Thurien metagranite found by Béchennec et al. (2001) and contemporaneous with dextral shearing along the NBSASZ. It is also identical to the U-Pb zircon emplacement age obtained recently on the southward Questembert granite by Tartèse et al. (2011b), which is contemporaneous with dextral shearing along the SBSASZ. This new U-Pb emplacement age obtained on the Lizio granite thus indicates that both branches of the SASZ were active at the same time around 315–320 Ma. However, it is younger and does not overlap with the whole rock Rb-Sr isochron age of 337 ± 13 Ma (2σ), previously considered as the emplacement age of the granite (whole rock Rb-Sr isochron, recalculated from the six data of Peucat et al., 1979 and the three data of Tartèse and Boulvais, 2010). So far, all the available geochronological data imply that the NBSASZ has been active from ca. 344 Ma (whole rock Rb-Sr isochron age of the Pontivy granite, Peucat et al., 1979) down to ca.

315 Ma. However, it would be interesting to get new zircon U-Pb data on the other granitic massifs emplaced along the NBSASZ. Indeed, the existing Rb-Sr isochron ages may be too old for these granites. Such old inherited "isochrons" have been described for example by Roddick and Compston (1977) for the crustally-derived Murrumbidgee Batholith, Australia. Moreover, whole rock-mineral isochrons on two samples from the Pontivy granite (whole rock Rb-Sr isochron age of 344 ± 8 Ma) yielded ages identical within error at 311 ± 9 and 310 ± 9 Ma respectively (Peucat et al., 1979), ages that are consistent with a Late Carboniferous emplacement for the Pontivy granite. We thus believe that the ca. 340 Ma old emplacement ages obtained through whole rock Rb-Sr dating of synkinematic granites along the NBSASZ are actually not emplacement ages of these granites but rather represent inherited "isochrons" in the sense of Roddick and Compston (1977). In that case, initiation of dextral shearing along the NBSASZ may not be as old as the ca. 340 Ma age that has been considered so far. Indeed, our data on the Lizio granite give a maximum age of 322 Ma for the activity along the NBSASZ.

$^{40}Ar/^{39}Ar$ dates obtained on muscovite grains from four samples of the Lizio granite range between 311.5 and 308.2 Ma. The two oldest dates are identical within error with the zircon U-Pb emplacement age of 316 ± 6 Ma and involve a subinstantaneous cooling of the intrusion, and the two other dates are slightly younger, considering the uncertainties associated with both techniques. This implies that either the younger muscovite grains have been affected by fluid-induced recrystallization processes after their magmatic isotopic closure (e.g. Villa, 2010) which would have reset the $^{40}Ar/^{39}Ar$ dates, or that the Lizio granite remained sufficiently warm during 2–3 Ma after its emplacement, above the argon closure temperature of muscovite. The muscovite chemistry
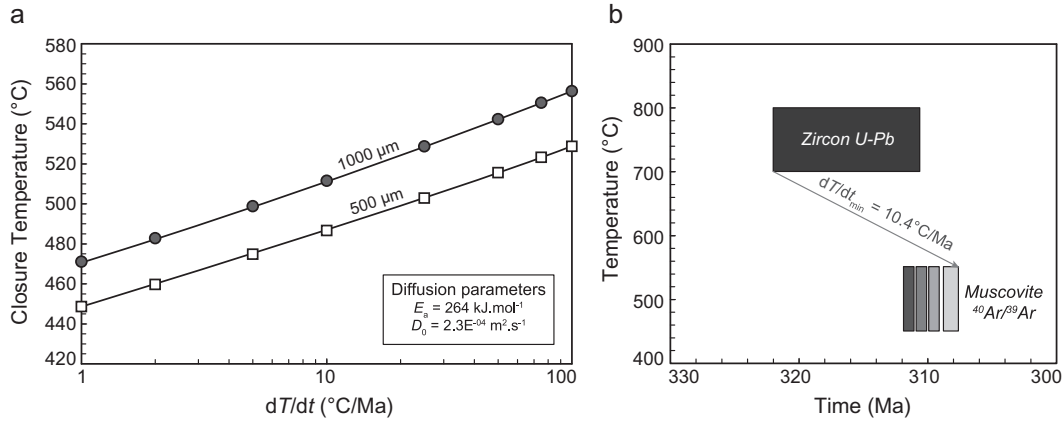
Fig. 7. (a) Computation of muscovite closure temperature (°C) for Ar diffusion against the cooling rate (°C/Ma) for diffusion radius of 0.5 and 1 mm. Parameters used are those of Harrison et al. (2009). (b) Temperature–Time plot for the Lizio granite.

Fig. 7. (a) Calcul de la température de fermeture (°C) pour la diffusion de l'Ar dans la muscovite en fonction du taux de refroidissement (°C/Ma), pour des domaines de diffusion de 0,5 et 1 mm. Les paramètres utilisés sont ceux de Harrison et al. (2009). b) Diagramme Température–Temps pour le granite de Lizio.

shows that all the muscovite grains have a typical primary magmatic composition, which likely precludes the first hypothesis of a fluids-induced recrystallization and resetting process. The closure temperature for argon in muscovite has for a long time been considered to be around 350 °C based in part on calibration of obtained ages vs. metamorphic grade (e.g. Purdy and Jäger, 1976). However, Harrison et al. (2009) recently published the first experimental study of argon diffusion in muscovite and showed that Ar retentivity in muscovite is greater than previously assumed. Based on their diffusion parameters (E_a = 264 kJ.mol^{-1}; D_0 = 2.3 E^{-04} m^2 s^{-1}), and taking 500 and 1000 μm for the diffusion radius, we have computed the different closure temperature as a function of cooling rates (Fig. 7a): the closure temperature ranges between ca. 450 and 550 °C, for the diffusion dimensions and cooling rates investigated. In a Temperature–Time diagram (Fig. 7b), the minimum cooling rate calculated considering U-Pb and ^{40}Ar/^{39}Ar ages and their associated uncertainties is 10.4 °C/Ma.

Taking the minimum zircon U-Pb age and the oldest muscovite dates corresponds to a subinstantaneous cooling of the granitic body. A simple 2D thermal numerical model (details in Appendix A) shows that a Lizio-type granitic pluton emplaced at mid-crustal depths cools down in less than 1 Ma (Fig. 8), consistently with this scenario. Conversely, a slow cooling rate of ca. 10 °C/Ma would imply

that the Lizio granite remained at a temperature above ca. 480–500 °C for a long time after its emplacement. The Lizio granite was emplaced around 4 kbar, which corresponds to a depth of 15 km considering only the lithostatic pressure and a granite density of 2.7. At this depth, temperatures of around 550 °C can be reached and maintained along continental strike-slip shear zones due to heat production by shear heating (Leloup et al., 1999). The cooling below the closure temperature of ca. 500 °C for such a slow cooling rate would have occurred when heat advection due to shear heating and therefore shearing along the NBSASZ had stopped. Moreover, one cannot totally rule out the influence of some fluid-rock interactions which would have disturbed ^{40}Ar/^{39}Ar age spectra without being recorded by the whole rock and muscovite chemistry. Indeed, the analyzed muscovite grains display subtle saddle-shaped ^{40}Ar/^{39}Ar age spectra that may indicate fluid-induced disturbance (e.g. Alexandrov et al., 2002; Cheilletz et al., 1999). Finally, to a first order, our new data are consistent with a simple cooling of the intrusion, with possible, but limited, influence of shear heating and fluid-rock interaction. A surprising result is the absence of consistency between the muscovite ^{40}Ar/^{39}Ar dates and the shearing gradients observes throughout the Lizio granite. This could result from the choice we made to
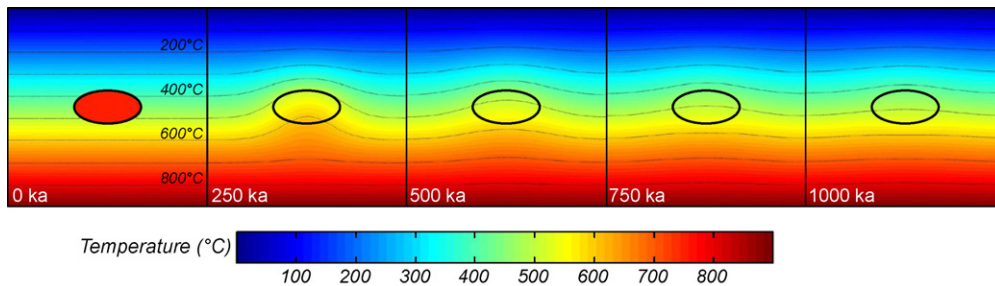

Fig. 8. 2D thermal modelling of the cooling of the Lizio granite during 1 Ma (see details in Appendix A).

Fig. 8. Modèle thermique 2D du refroidissement du granite de Lizio pendant 1 Ma (voir les détails dans l'Annexe A).

date large muscovite phenocrysts in all the samples. It would deserve further studies, notably dating increasingly deformed micas toward the NBSASZ to better evaluate if potential postemplacement events have affected the K-Ar system in micas.

6. Conclusion

Zircon U-Pb dating carried out on the Lizio granite yielded an age of 316 ± 6 Ma that is interpreted as the emplacement age of the granite, and therefore also of dextral shearing along the northern branch of the SASZ. This is significantly younger than the previous ca. 340 Ma whole rock Rb-Sr age interpreted as dating the emplacement of the Lizio granite. The significance of this older age is not yet well understood and it should therefore be treated with caution. $^{40}Ar/^{39}Ar$ analyses performed on various muscovite grains from the Lizio granite yielded dates of 311.5–308.2 Ma. As geochemical evidence precludes late fluids-induced large perturbations of the K-Ar isotopic system in muscovite, these dates likely reflect cooling ages below the argon closure temperature. Two extreme scenarios may explain the obtained ages, either a subinstantaneous cooling of the granite, or conversely, a very slow cooling which lasted several millions of years. This last scenario requires that the Lizio granite remained in a hot environment for a long time after its emplacement. This could have been caused by shear heating due to dextral shearing along the northern branch of the SASZ.

Acknowledgments

Appendix A. Appendix A: 2D thermal numerical model

The 2D thermal code used in this study solves the heat diffusion equation (A.1):

$$\rho C_p \frac{\partial T}{\partial t} = k \nabla^2 T + Hr \tag{A.1}$$

where ρ, C_p and k are material density, specific heat capacity and thermal conductivity, respectively and Hr corresponds to the radiogenic heat production. This equation is solved numerically in the implicit formulation using the finite difference method. In this study, the heat production (Hr) is set to zero. Indeed, preliminary tests have been done with values from 1 to 5 $\mu W.m^{-3}$ and the results show that results are not significantly different after 1 Myr of experiment. The initial setup is displayed in the Fig. A1. The granitic intrusion is modelled as an ellipse (5 km high and 10 km long) located at 15 km depth in a host rocks medium with a linear thermal
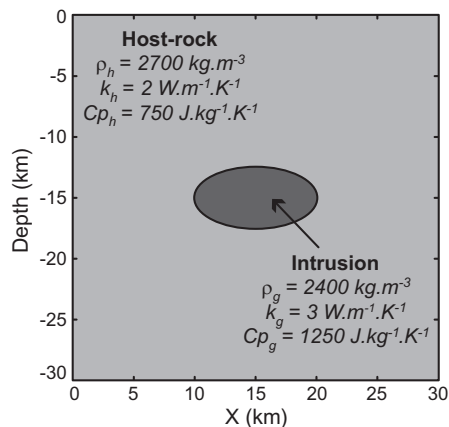

Fig. A1. Initial setup used for the 2D thermal modelling.

Fig. A1. Configuration initiale utilisée pour le modèle thermique 2D.

gradient of 30 °C km^{-1}. The resolution used is 151 × 151 nodes (i.e., 200 m).

References

Alexandrov, P., Ruffet, G., Cheilletz, A., 2002. Muscovite recrystallization and saddle-shaped $^{40}Ar/^{39}Ar$ age spectra: Example from the Blond granite (Massif Central, France). Geochim. Cosmochim. Acta 66, 1793–1807.

Ballèvre, M., Bosse, V., Ducassou, C., Pitra, P., 2009. Palaeozoic history of the Armorican Massif: Models for the tectonic evolution of the suture zones. C. R. Geoscience 341, 174–201.

Bea, F., Montero, P., González-Lodeiro, F., Talavera, C., 2007. Zircon inheritance reveals exceptionally fast crustal magma generation processes in Central Iberia during the Cambro-Ordovician. J. Petrol. 48, 2327–2339.

Béchennec, F., Hallégouët, B., Thiéblemont, D., 2001. Rosporden 1/50000 geological map manual (347). BRGM, Orléans, France.

Bernard-Griffiths, J., Peucat, J.J., Sheppard, S., Vidal, P., 1985. Petrogenesis of Hercynian leucogranites from the southern Armorican Massif: contribution of REE and isotopic (Sr, Nd, Pb and O) geochemical data to the study of source rock characteristics and ages. Earth Planet. Sci. Lett. 74, 235–250.

Berthé, D., 1980. Le Cisaillement Sud Armoricain dans la région de St. Jean Brévelay (Morbihan). Analyse de la déformation cisaillante. Unpublished Ph.D. Thesis, University of Rennes 1, France.

Berthé, D., Choukroune, P., Jégouzo, P., 1979. Orthogneiss, mylonite and non coaxial deformation of granites - Example of the South Armorican Shear Zone. J. Struct. Geol. 1, 31–42.

Brown, M., Dallmeyer, R.D., 1996. Rapid Variscan exhumation and the role of magma in core complex formation: southern Brittany metamorphic belt, France. J. Metamorph. Geol. 14, 361–379.

Cheilletz, A., Ruffet, G., Marignac, C., Kolli, O., Gasquet, D., Féraud, G., Bouillin, J.P., 1999. $^{40}Ar/^{39}Ar$ dating of shear zones in the Variscan basement of the Greater Kabylia (Algeria). Evidence of an Eo-Alpine event at 128 Ma (Hauterivian–Barremian boundary): geodynamic consequences. Tectonophysics 306, 97–116.

Cherniak, D.J., Watson, E.B., 2001. Pb diffusion in zircon. Chem. Geol. 172, 5–24.

Gapais, D., 1989. Shear structures within deformed granites: mechanical and thermal indicators. Geology 17, 1144–1147.

Gapais, D., Lagarde, J.L., Le Corre, C., Audren, C., Jégouzo, P., Casas Sainz, A., Van Den Driessche, J., 1993. La zone de cisaillement de Quiberon : témoin d'extension de la chaîne varisque en Bretagne méridionale au Carbonifère. C. R. Acad. Sci. Paris. Ser. IIa 316, 1123–1129.

Gloaguen, E., Branquet, Y., Boulvais, P., Moëlo, Y., Chauvel, J.J., Chiappero, P.J., Marcoux, E., 2007. Palaeozoic oolitic ironstone of the French Armorican Massif: a chemical and structural trap for orogenic base metal-As-Sb-Au mineralisation during Hercynian strike-slip deformation. Miner. Deposita 42, 399–422.

Gumiaux, C., Gapais, D., Brun, J.P., Chantraine, J., Ruffet, G., 2004. Tectonic history of the Hercynian Armorican Shear belt (Brittany. France). Geodin. Acta 17, 289–307.

Harrison, T.M., Aleinikoff, J.N., Compston, W., 1987. Observations and controls on the occurrence of inherited zircon in Concord-type granitoids. New Hampshire. Geochim. Cosmochim. Acta 51, 2549–2558.

Harrison, T.M., Célérier, J., Aikman, A.B., Hermann, J., Heizler, M.T., 2009. Diffusion of ^{40}Ar in muscovite. Geochim. Cosmochim. Acta 73, 1039–1051.

Jackson, S.E., Pearson, N.J., Griffin, W.L., Belousova, E.A., 2004. The application of laser ablation-inductively coupled plasma-mass spectrometry to in situ U-Pb zircon geochronology. Chem. Geol. 211, 47–69.

Jégouzo, P., 1980. The South Armorican Shear Zone. J. Struct. Geol. 2, 39–47.

Jégouzo, P., Rossello, E.A., 1988. La Branche Nord du Cisaillement Sud–Armoricain (France) : un essai d'évaluation du déplacement par l'analyse des mylonites. C. R. Acad. Sci. Paris, Ser. IIa 307, 1825–1831.

Košler, J., Sylvester, P.J., 2003. Present trends and the future of zircon in geochronology: laser ablation ICPMS. In: Hanchar, J.M., Hoskin, P.W.O. (Eds.), Zircon. Rev. Mineral. Geochem. 53, 243–275.

Košler, J., Fonneland, H., Sylvester, P., Tubrett, M., Pedersen, R.B., 2002. U-Pb dating of detrital zircons for sediments provenance studies–a comparison of laser ablation ICPMS and SIMS techniques. Chem. Geol. 182, 605–618.

Košler, J., Forst, L., Sláma, J., 2008. Lamdate and Lamtool: spreadsheet-based data reduction for laser ablation ICP-MS. In: Sylvester, P. (Ed.), Laser Ablation ICP-MS in the Earth Sciences: Current Practices and Outstanding Issues. Mineralogical Association of Canada, Short Course Series, 40. pp. 315–317.

Le Corre, C., Auvray, B., Ballèvre, M., Robardet, M., 1991. Le Massif Armoricain. Sciences Géologiques 44, 31–103.

Leloup, P.H., Ricard, Y., Battaglia, J., Lacassin, R., 1999. Shear heating in continental strike-slip shear zones: model and field examples. Geophys. J. Int. 136, 19–40.

Lemarchand, J., Boulvais, P., Gaboriau, M., Boiron, M.C., Tartèse, R., Cokkinos, M., Bonnet, S., Jégouzo, P., 2011. Giant quartz vein formation and high elevation meteoric fluid infiltration into the South Armorican Shear Zone: geological, fluid inclusion and stable isotope evidence. J. Geol. Soc. London, in press. doi:10.1144/0016-76492010-186.

Ludwig, K.R., 2008. Isoplot/Ex version 3.70: A geochronological toolkit for Microsoft Excel. Berkeley Geochronology Center, Special Publication 4, 73 p.

Miller, C.F., Stoddard, E.F., Bradfish, L.J., Dollase, W.A., 1981. Composition of plutonic muscovite; genetic implications. Can. Mineral. 19, 25–34.

Miller, C.F., McDowell, S.M., Mapes, R.W., 2003. Hot and cold granites? Implications of zircon saturation temperatures and preservation of inheritance. Geology 31, 529–532.

Pattison, D.R.M., Tracy, R.J., 1991. Phase equilibria and thermobarometry of metapelites. In: Kerrich, D.M. (Ed.), Contact Metamorphism. Rev. Mineral. Geochem., 26. pp. 105–206.

Pattison, D.R.M., Spear, F.S., Cheney, J.T., 1999. Polymetamorphic origin of muscovite + cordierite + staurolite + biotite assemblages: implications for the metapelitic petrogenetic grid and for P-T paths. J. Metamorph. Geol. 17, 685–703.

Peucat, J.J., Charlot, R., Mifdal, A., Chantraine, J., Autran, A., 1979. Définition géochronologique de la phase bretonne en Bretagne centrale.

Étude Rb/Sr de granites du domaine Centre-Armoricain. Bull. B. R. G. M. 4, 349–356.

Pitra, P., Boulvais, P., Antonoff, V., Diot, H., 2008. Wagnerite in a cordierite-gedrite gneiss: witness of long-term fluid-rock interaction in the continental crust (Ile d'Yeu, Armorican Massif, France). Am. Mineral. 93, 315–326.

Purdy, J.W., Jäger, E., 1976. K-Ar ages on rock-forming minerals from the Central Alps. Mem. Inst. Geol. Min. Univ. Padova 30 .

Renne, P.R., Swisher, C.C., Deino, A.L., Karner, D.B., Owens, T.L., DePaolo, D.J., 1998. Intercalibration of standards, absolute ages and uncertainties in ^{40}Ar/^{39}Ar dating. Chem. Geol. 145, 117–152.

Roddick, J.C., Bevier, M.L., 1995. U-Pb dating of granites with inherited zircon: Conventional and ion microprobe results from two Paleozoic plutons, Canadian Appalachians. Chem. Geol. 119, 307–329.

Roddick, J.C., Compston, W., 1977. Strontium isotopic equilibration: a solution to a paradox. Earth Planet. Sci. Lett. 34, 238–246.

Ruffet, G., Féraud, G., Amouric, M., 1991. Comparison of ^{40}Ar/^{39}Ar conventional and laser dating of biotites from the North Tregor batholiths. Geochim. Cosmochim. Acta 55, 1675–1688.

Ruffet, G., Féraud, G., Ballèvre, M., Kienast, J.R., 1995. Plateau ages and excess argon in phengites - An Ar-40-Ar-39 laser probe study of alpine micas (Sesia zone, Western Alps, northern Italy). Chem. Geol. 121, 327–343.

Sláma, J., Košler, J., Condon, D.J., Crowley, J.L., Gerdes, A., Hanchar, J.M., Horstwood, M.S.A., Morris, G.A., Nasdala, L., Norberg, N., Schaltegger, U., Schoene, B., Tubrett, M.N., Whitehouse, M.J., 2008. Plešovice zircon - a new natural reference material for U-Pb and Hf isotopic microanalysis. Chem. Geol. 249, 1–35.

Tartèse, R., Boulvais, P., 2010. Differentiation of peraluminous leucogranites "en route" to the surface. Lithos 114, 353–368.

Tartèse, R., Boulvais, P., Poujol, M., Chevalier, T., Paquette, J.L., Ireland, T.R., Deloule, E., 2011a. Mylonites of the South Armorican Shear Zone: Insights for crustal-scale fluid flow and water–rock interaction processes. J. Geodyn., in press. doi:10.1016/j.jog.2011.05.003.

Tartèse, R., Boulvais, P., Poujol, M., Gloaguen, E., 2011b. The Late Carboniferous Variscan evolution of the Armorican Massif (France): magmatism, hydrothermalism and metallogenic consequences. Geophys. Res. Abstr. 13, 2422.

Turrillot, P., Augier, R., Faure, M., 2009. The top-to-the-southeast Sarzeau shear zone and its place in the late-orogenic extensional tectonics of southern Armorica. Bull. Soc. Geol. France 180, 247–261.

Villa, I.M., 2010. Disequilibrium textures versus equilibrium modelling: geochronology at the crossroads. In: Spalla, M.I., Marotta, A.M., Grosso, G. (Eds.), Advances in Interpretation of Geological Processes: Refinement of Multi-scale Data and Integration in Numerical Modelling. Geol. Soc. London Spec. Pub., 332. pp. 1–15.

Wiedenbeck, M., Alle, P., Corfu, F., Griffin, W.L., Meier, M., Oberli, F., von Quadt, A., Roddick, J.C., Spiegel, W., 1995. Three natural zircon standards for U-Th-Pb, Lu-Hf, trace element and REE analyses. Geostandard. Newslett. 19, 1–23.

Whitney, D.L., Evans, B.W., 2010. Abbreviations for names of rock-forming minerals. Am. Mineral. 95, 185–187.